

# CFD modeling of an ion-drag micropump

J. Darabi\*, C. Rhodes

*Department of Mechanical Engineering, University of South Carolina, Columbia SC 29208, USA*

Received 18 February 2005; received in revised form 21 October 2005; accepted 26 October 2005

Available online 6 December 2005

## Abstract

A two-dimensional numerical simulation study has been performed to model an electrohydrodynamic (EHD) micropump. The micropump consists of an array of interdigitated electrodes along the top and bottom of the micropump channel. The focus of the simulations was to study the effects of electrode gap, stage gap, channel height, and applied voltage. The numerical results were first validated with experimental data and then applied to obtain optimum electrode design and pump characteristics curves for geometries of interest. Additionally, the simulation results provide details about the flow behavior of the micropump and clearly capture local flow induced by EHD forces.

© 2005 Elsevier B.V. All rights reserved.

*Keywords:* Electrohydrodynamic micropump; Ion-drag; EHD; CFD modelling; Simulation

## 1. Introduction

With the development of microfabrication technology, intense research efforts have been made towards microfluidic systems and microliquid handling devices. Micropumps are one of the crucial components for moving liquids in the miniaturized systems. Their compact size and ability to handle very small and precise volumes of liquid make them attractive for applications in microfluidic systems, biotechnology, microchemical analysis systems, drug delivery systems, and chip-integrated cooling systems. In the past decade, a large number of micropumps have been developed to deliver and transport a wide range of liquids. These micropumps produce a flow rate ranging from a few  $\mu\text{l}/\text{min}$  to  $\text{ml}/\text{min}$ , and a pressure varying from a few Pa to several hundred kPa or more.

Micropumps can be classified into two groups: mechanical micropumps (with moving parts) and non-mechanical micropumps (without moving parts). Some examples of mechanical micropumps include but are not limited to thermopneumatically driven peristaltic pumps, electrostatically driven reciprocating pumps, piezoelectric micropumps, and shape memory alloy micropumps. Non-mechanical micropumps use a variety of electric-fluid interactions to generate forces in the liquid, such as electrokinetic micropumps, magnetohydrodynamic micropumps,

and electrohydrodynamic micropumps. As with many technologies, each method has its advantages and disadvantages that depend upon the particular application. A comprehensive overview of micropumps is given elsewhere [1–3]. Since the focus of this paper is on ion-drag EHD micropumps, only micropumps working based on this principle will be discussed in the following.

The ion-drag EHD pumping uses the interaction of an electric field with electric charges, dipoles or particles embedded in a dielectric fluid to move the fluid. The charges can be injected into liquid by field emission or field ionization processes. The main driving force in ion-drag pumps is the movement of ions across an imposed electric field. The electric field is established between a charged electrode called an emitter and a grounded electrode called a collector. The Coulomb force that is produced by an external electrical field acts on all charges in the fluid. The friction between the moving ions and the working fluid drags the working fluid towards the collector, thus setting the fluid in motion.

The fact that dielectric liquids can be pumped by the injection of ions in an applied electric field has been known for quite some time. Indeed, the theoretical and experimental investigations of the EHD pump were widely pursued in early 1960s. Stuetzer [4,5] and Pickard [6,7] were among the first who proposed and studied the ion-drag EHD pumping. Later, many researchers [8–28] made further studies of the ion-drag EHD pump. Most of these studies, however, have been focused on experimental and/or theoretical investigations. This paper presents a

\* Corresponding author. Tel.: +1 803 777 8013; fax: +1 803 777 0106.  
E-mail address: [darabi@engr.sc.edu](mailto:darabi@engr.sc.edu) (J. Darabi).

**Nomenclature**

<i>d</i>	gap between electrodes (m)
<i>E</i>	electric field strength (V/m)
<i>f</i>	force density (N/m <sup>3</sup> )
<i>g</i>	gap between two neighboring stages (m)
<i>h</i>	pressure head (m)
<i>k</i>	dielectric constant
<i>I</i>	current (A)
<i>J</i>	current density (A/m <sup>2</sup> )
<i>m</i>	mass (kg)
<i>P</i>	pressure (Pa)
<i>t</i>	time (s)
<i>u</i>	velocity (m/s)
<i>V</i>	voltage (V)

*Greek symbols*

$\epsilon$	permittivity (F/m)
$\epsilon_0$	permittivity of vacuum
$\eta$	dynamic viscosity (Ns/m <sup>2</sup> )
$\mu$	mobility (m <sup>2</sup> /V s)
$\rho_c$	charge density (C/m <sup>3</sup> )
$\rho_m$	mass density (kg/m <sup>3</sup> )
$\sigma$	electric conductivity (1/ $\Omega$ m)
$\tau$	shear stress (N/m <sup>2</sup> )
$\phi$	potential field (V)

numerical investigation to study EHD pumping by solving governing equations with simplifications based on experimental observation.

EHD pumping is a complex phenomenon involving the interaction between fluid flow and electric fields. Theoretical modeling of this process is nearly impossible unless a number of simplified and somewhat unrealistic assumptions are made.

Most of the theoretical models developed thus far are simple, one-dimensional models and essentially relate the pumping pressure to the applied voltage or electric field only [4–7,9,13]. These models are unable to provide a detailed flow characteristics induced by the highly complex EHD phenomenon. Thus, the motivation for the present work is to perform a two-dimensional numerical investigation to study EHD pumping. This is essential to resolve the difference between theory and experiment and to improve the understanding of the fundamental mechanisms underlying the EHD pumping. The simulation of EHD pumping presented here is believed to be the first published work to numerically model EHD pumping. The simulation results provide details about the flow behavior and clearly capture local flow induced by EHD forces, which cannot be easily obtained from experimental or theoretical results.

The mechanism of ion-drag pumping between a pair of emitter and collector electrodes is schematically demonstrated in Fig. 1. As shown in Fig. 1a, some impurities may be initially present in the liquid. When the voltage is turned on, these impurities are attracted towards the opposite electrodes (step b). This process is short and stops when these charges are neutralized at the electrodes. If the voltage is further increased until the electric field around the tip of the saw-tooth emitter exceeds certain threshold strength, electrons will be emitted from the emitter electrode into the dielectric liquid (step c). Next, negative ions are produced by electron attachment to liquid molecules represented by  $M^-$  and  $[M]_n^-$  (step d). These negative ions will then move towards the positive electrode. With comparative mass and low mobility, these negative ions will exert a drag force on surrounding molecules and create a fluid flow (step e).

Fig. 2 shows a top view of an electrode pattern used in the model. A detailed description of the micropump and experimental results are given in earlier publications of the first author [21,28]. The micropump had an overall dimension of 16 mm × 28 mm × 1.05 mm. Each emitter electrode had a width of 9.3  $\mu$ m and the collector electrode consisted of a planar

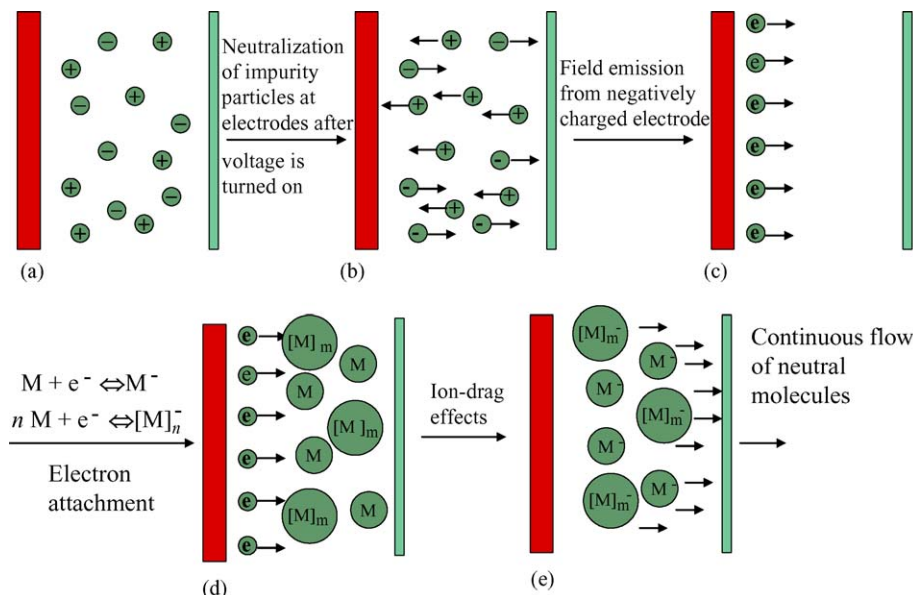


Fig. 1. Pumping mechanism in an ion-drag micropump.

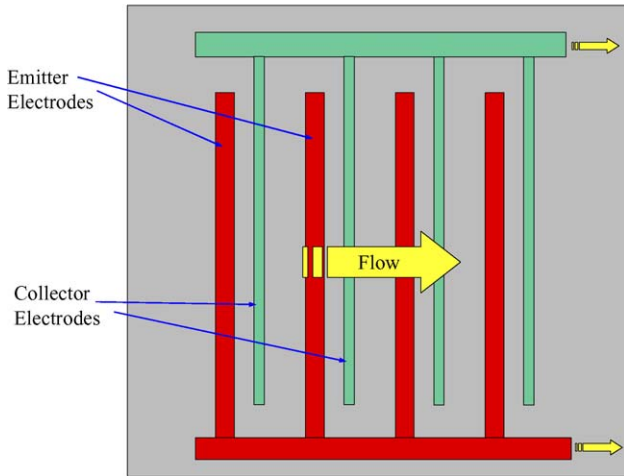


Fig. 2. A top view of an interdigitated electrode pattern.

electrode with a width of  $5 \mu\text{m}$ . The gap between the emitter and collector electrodes was  $10 \mu\text{m}$ . The distance between each neighboring stage (a pair of emitter and collector electrodes) was  $20 \mu\text{m}$ . Microscale EHD pumps offer the advantages of working under reduced voltage compared to their macroscale counterparts due to very small gaps between electrodes.

## 2. Computational approach

A two-dimensional numerical model was performed using commercial CFD software FIDAP to model EHD pumping between an array of emitter and collector electrodes. The numerical models was first validated with experimental data and then applied to obtain optimum electrode design and operating conditions for geometries of interest. Fig. 3 depicts a schematic diagram of the physical model used in the simulation. As shown in Fig. 3,  $g$  and  $d$  are the gap between electrodes and the gap between two neighboring stages, respectively. Since the geometry exhibits periodic repetition, it is more economical to solve a representative portion of flow field rather than the entire domain.

In order to formulate a mathematically tractable problem, we consider two-dimensional flow passing inside a channel. The governing equations are the mass, momentum and charge equations:

- Conservation of mass:

$$\frac{\partial \rho_m}{\partial t} + \frac{\partial(\rho_m u_j)}{\partial x_j} = 0 \quad (1)$$

- Conservation of momentum:

$$\frac{\partial(\rho_m u_i)}{\partial t} + \frac{\partial(\rho_m u_i u_j)}{\partial x_j} = -\frac{\partial P}{\partial x_i} + \frac{\partial \tau_{ij}}{\partial x_j} + \rho_m f_i + \rho_c E \quad (2)$$

where  $P$  is the pressure,  $\tau$  the shear stress,  $f_i$  the body force and the last term is the Coulomb force. The electric field can be written as

$$E = -\frac{\partial \phi}{\partial x_i} \quad (3)$$

where  $\phi$  is the potential field.

- Conservation of charge:

$$\frac{\partial \rho_c}{\partial t} + \nabla \cdot J = 0 \quad (4)$$

where  $J$  is the current flux. The current flux is composed of flux due to convection of charge, flux due to diffusion and flux due to ionic mobility components.  $J$  may be written as

$$J = \rho_c u + \sigma E + \rho_c \mu E \quad (5)$$

Substituting the divergence of Eq. (5) into (4), we obtain

$$\frac{\partial \rho_c}{\partial t} + \nabla \cdot (\rho_c u) + \nabla \cdot (\sigma E) + \nabla \cdot (\rho_c \mu E) = 0 \quad (6)$$

### 2.1. Gauss's law

The Gauss law describes the relationship between charge density and electric field and is given by

$$\nabla \cdot (\varepsilon E) = \rho_c \quad (7)$$

The assumptions are as follows:

- laminar, steady and incompressible flow;
- the electrodes are planar strips on the bottom substrate;
- the end effect at two ends of the channel is negligible;
- only one type of ion is present in the liquid.

The boundary conditions for the potential field and the charge concentration are of Dirichlet type, which requires the values of the potential field and charge concentration. The flow field

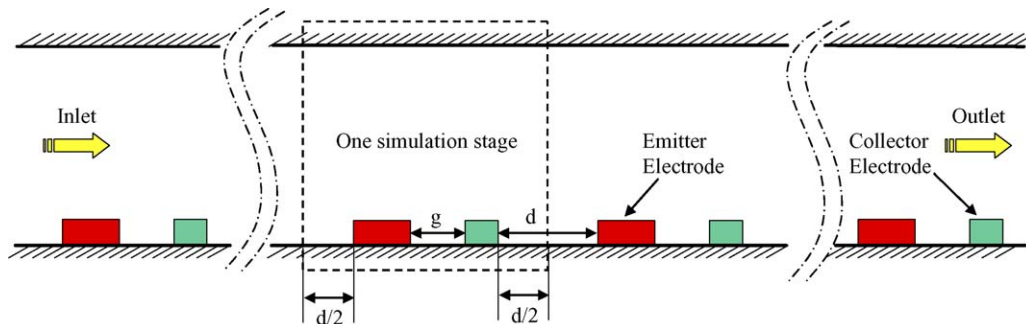


Fig. 3. A schematic diagram of the physical model.

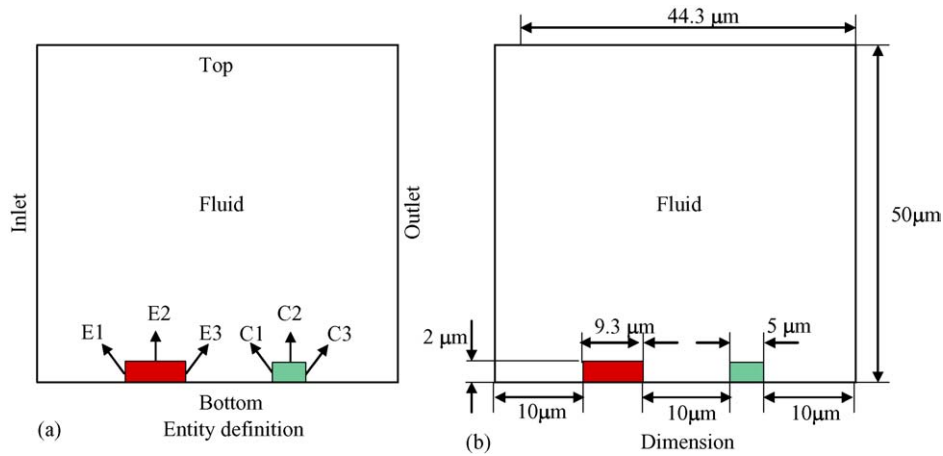


Fig. 4. Entity definition and dimensions of the model: (a) entity definition; (b) dimension.

exhibits spatial periodicity. At the midpoint between two adjacent stages, both the geometry and boundary conditions exhibit periodic characteristics. Thus, only a segment of the whole domain was simulated. Fig. 4 shows the entity definition and dimensions of the model. Boundary conditions are specified through defining entities in the model. Periodic boundary conditions were applied to the representative segment by requiring that the solution at some point on the boundary be the same as the solution at another point on the boundary. The numerical solution is based on a finite element method (FEM). Extensive trial runs were performed prior to main simulations to ensure that the solution was grid independent.

**3. Results and discussion**

The complete analysis of the EHD pumping mechanism requires the solution of both the electric field and charge density distributions, given by coupled equations (6) and (7). The solution of these equations is not straightforward due to the

absence of a known boundary condition for the charge density. One approach is to estimate the charge density from the measured current during the experiments, but this still requires several assumptions regarding the ionization region at the emitter and the charge behavior inside the computational domain. The solution strategy that has been employed by the authors was to compute the charge density due to the electric field effect inside the computational domain assuming that the flow field and the charge transport do not significantly interact. The computed charge density was then applied as boundary condition to obtain new electric field. The iteration was repeated until the difference between the computed charge density in two subsequent iterations value was less than a specified value. The focus of the simulations was to study the effects of channel height, electrode gap (g), stage gap (d), applied voltage ( $\phi$ ), and d/g ratio. A summary of these findings will follow.

Figs. 5–7 depict representative simulation results that show potential field, velocity vector plots, and pressure contour plots between a pair of emitter and collector electrodes in a

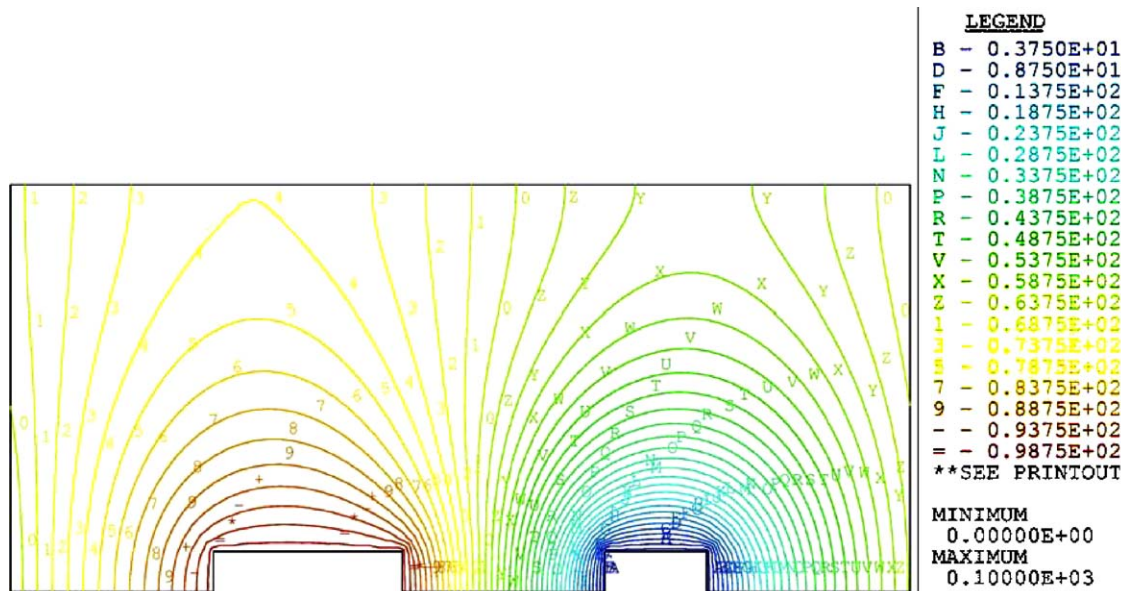


Fig. 5. A representative local potential field.

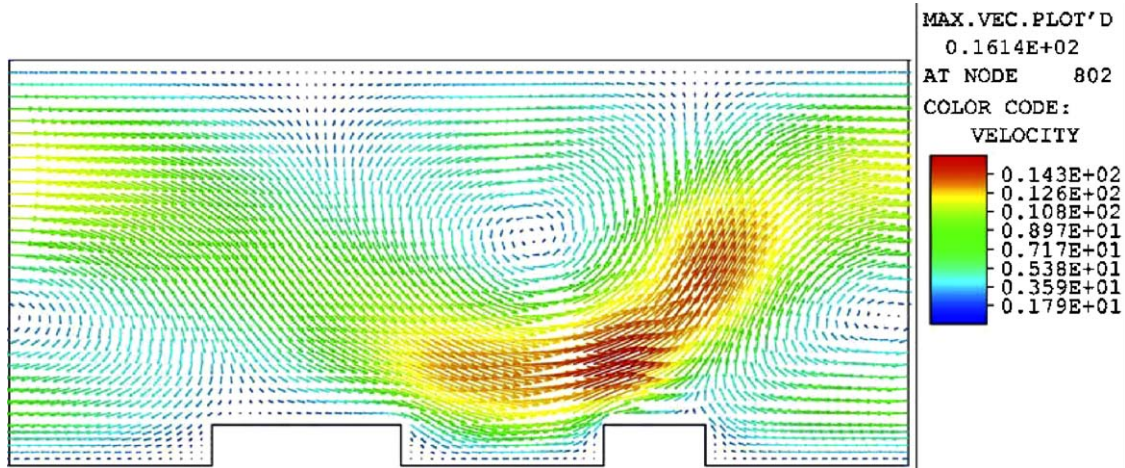


Fig. 6. A representative local velocity profile.

micropump with a channel height of 20  $\mu\text{m}$ . The working fluid is HFE-7100 thermal fluid (3M, St. Paul, MN). The potential field is shown in Fig. 5. The emitter electrode is charged and the collector electrode is grounded. Fig. 6 depicts the local flow induced by EHD forces from an emitter electrode towards a collector electrode. These plots also show a small back flow from the emitter of the second stage toward the collector of the first stage (right to left). However, since the distance between two neighboring stages ( $d$ ) is twice that of the gap between emitter and collector electrode of each stage ( $g$ ), the backflow is weaker and the net pumping flow is still from left to right. This behavior reflects a physical fact that the strongest driving force occurs between the electrodes. Local pressure contour plots are shown in Fig. 7. The pressure generated within one stage was calculated from the difference between the average pressure at the inlet and outlet of the representative segment. A total generated pressure was then obtained by multiplying the number of stages by the pressure generated from one stage.

The effects of pressure on the local velocity vector plots are shown in Fig. 8. The electric body force, acting on the ions, drags the liquid molecules between the electrodes. At zero pressure, a weak counter-clockwise rotational flow is observed in the region above the electrodes. The flow between electrodes becomes more rotational with increasing the pressure. As the generated pressure is further increased, these regions of rotational flow grow and eventually evolve into larger rotational regions that spread over the entire cross-section of the channel. Note that two vortices can be observed: a strong counter-clockwise vortex in the region above the electrodes and a weak vortex in the region between two neighboring stages. The latter is faded away as the  $d/g$  ratio increases.

In order to verify the simulation results, a micropump with a  $d/s$  ratio of 2 at a channel height of 50  $\mu\text{m}$  was designed, fabricated and tested. A detailed description of the micropump fabrication and experimental set-up is available in earlier publications of the first author [21,28] and thus, it is not repeated

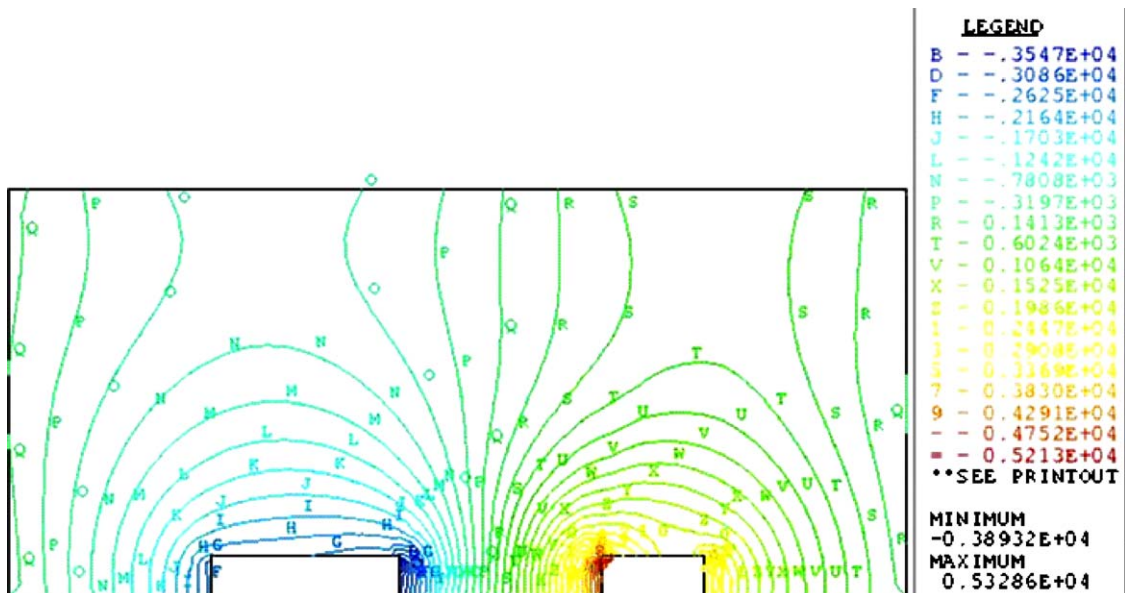


Fig. 7. A representative local pressure contour.

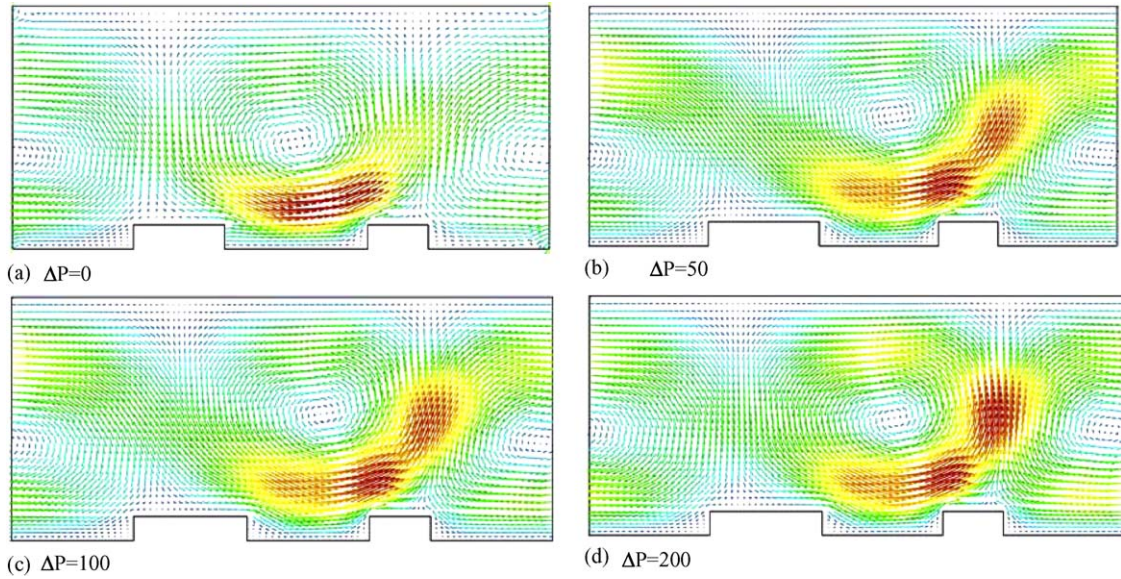


Fig. 8. Local velocity profiles at various pressures for a channel height of 20  $\mu\text{m}$  with bottom electrode.

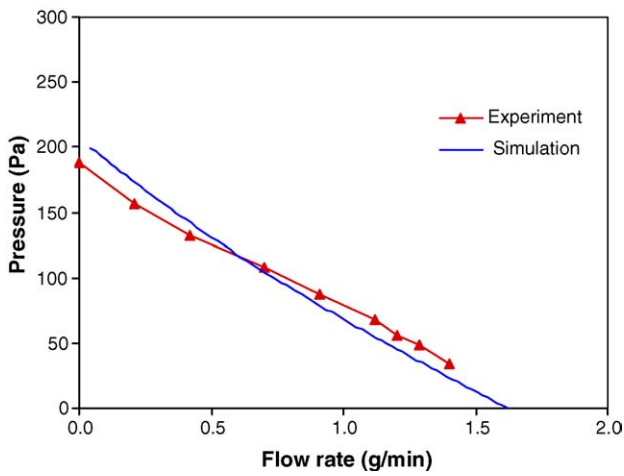


Fig. 9. A comparison between the simulation and experiment [28].

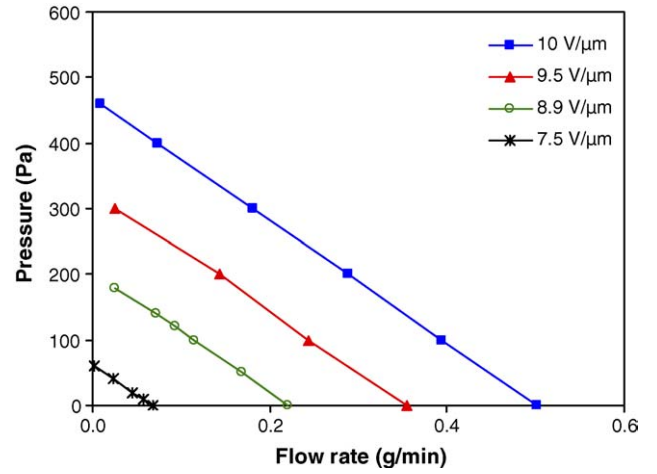


Fig. 11. Pressure vs. mass flow rate at various electric fields for a channel height of 20  $\mu\text{m}$ .

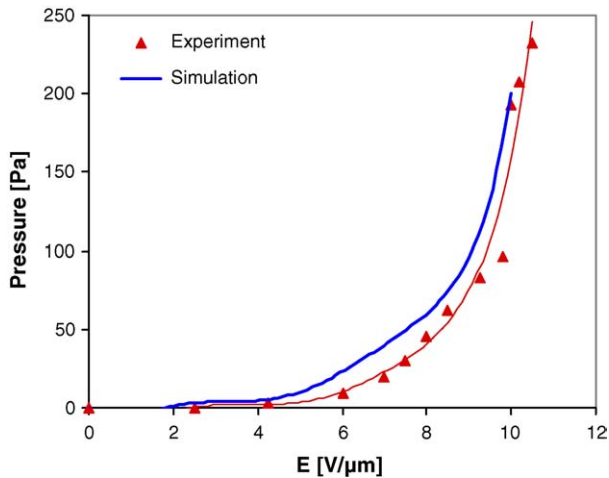


Fig. 10. A comparison between simulated and measured pressure head as a function of electric field under no flow condition [28].

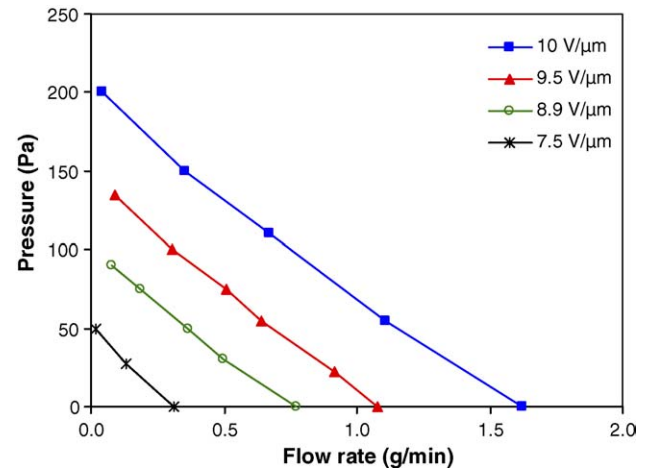


Fig. 12. Pressure vs. mass flow rate at various electric fields for a channel height of 50  $\mu\text{m}$ .

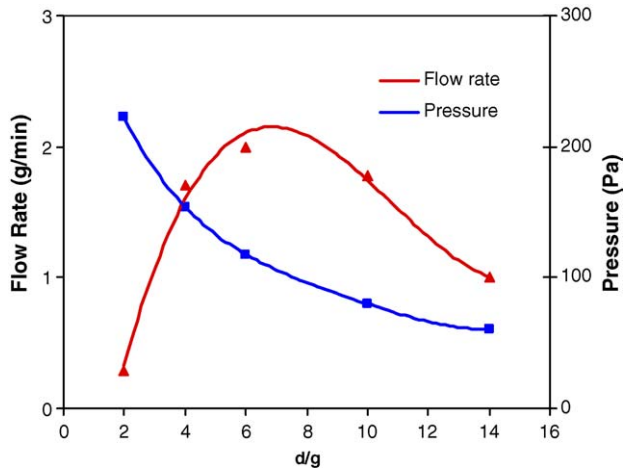


Fig. 13. Effects of d/g on flow rate and pressure.

of 20 and 50  $\mu\text{m}$ . The results show a nearly linear relationship between the flow rate and pressure. This is due to the fact that flow inside the channel is laminar and the flow rate is basically a linear function of the pressure in laminar flows. These performance curves indicate linear reduction in flow rate as the pressure increases. Under a specified pressure, the flow rate increases as the channel height increases.

An important parameter that affects the flow rate and pressure is the ratio of the gap between stages ( $d$ ) to the gap between the electrodes ( $g$ ). Fig. 13 depicts simulation results as a function d/g ratio for a constant electrode gap ( $g$ ) of 10  $\mu\text{m}$  and a channel height of 50  $\mu\text{m}$ . The results indicate that the flow rate initially increases with increasing d/g ratio, reaches a maximum, and then decreases. This indicates that there is an optimum d/g ratio at which the flow rate is maximum. The initial increase in flow rate is due to the fact that the backflow between stages decrease with increasing d/g ratio. However, as d/g ratio is further increased, the internal frictional losses increase, leading to a reduced flow rate. The results also indicate that there is a significant decrease in the generated pressure as d/g increases. This is because the total number of stages per unit length decreases with increasing d/g ratio. Thus, the decrease in the total generated pressure is due to the decreased number of stages.

in the present paper for sake of brevity. Figs. 9 and 10 show comparisons between experimental and simulation results. The agreement between numerical predictions and experimental data is quite good.

Figs. 11 and 12 depict the variation of the flow rate and pressure at various electric field strengths for two channel heights

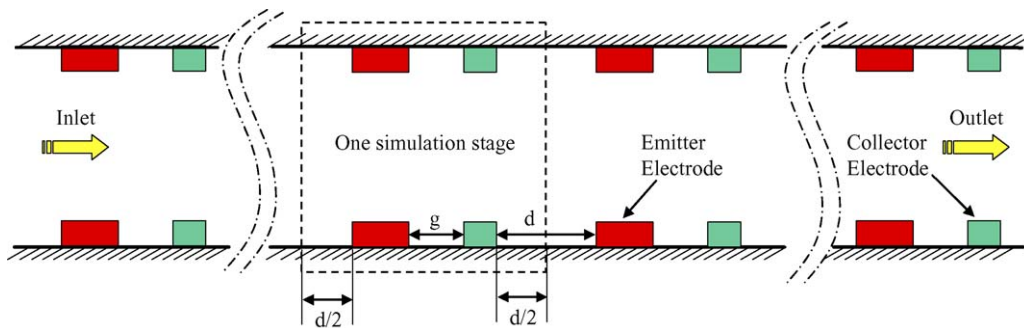


Fig. 14. A schematic diagram of a micropump with top and bottom electrodes.

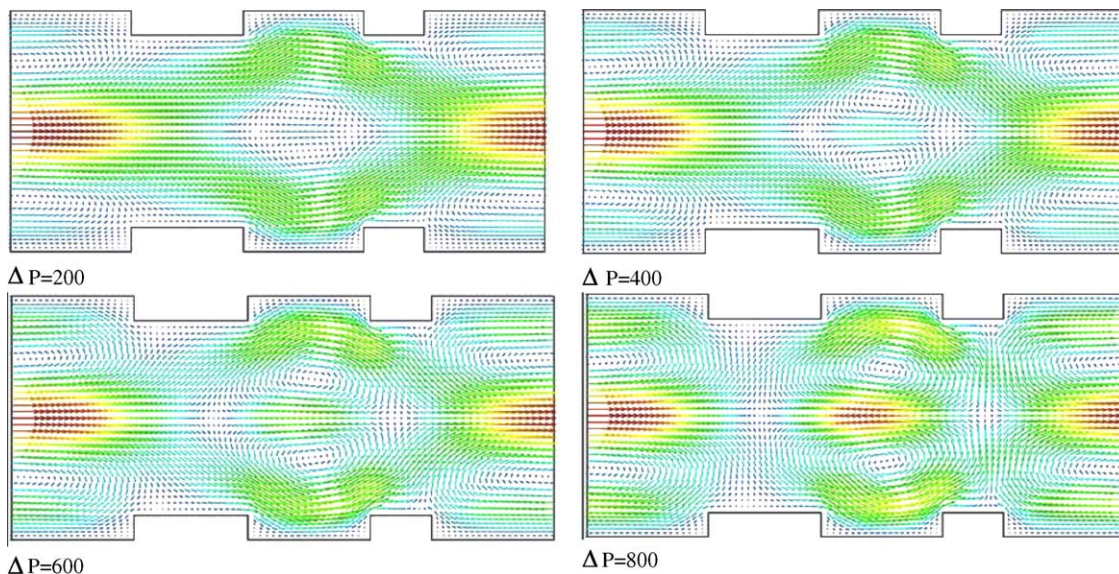


Fig. 15. Local velocity profiles at various pressures for a channel height of 20  $\mu\text{m}$  with top and bottom electrodes.

#### 4. Top and bottom electrodes

Simulation runs were also performed in order to investigate the effect of using an array of electrodes facing each other along the top and bottom of the micropump channel. Fig. 14 shows a schematic diagram for this configuration. All electrode dimensions are the same as those for a micropump with electrodes along the bottom wall. Figs. 15 and 16 illustrate local velocity vector plots at various pressures for two channel heights of 20 and 50  $\mu\text{m}$ , respectively. As expected, the velocity profile is symmetric along the horizontal centerline. The flow enters in the middle of the channel and splits into two symmetric streams as it goes over the electrodes. It is recombined in the region between two neighboring stages. Backflows are also observed near top and bottom walls from the emitter electrode toward the collector of the preceding stage. This pattern is repeated many times along the channel. At low pressures, two weak vortices are observed in

the region above the electrodes. As the pressure increases, these vortices grow and eventually evolve into two circulation loops that spread over the top and bottom halves of the channel. Four vortices can be observed for this configuration: two vortices in the region above the electrodes and two weak vortices in the region between two neighboring stages. The former becomes stronger as the pressure increases, eventually resulting in a net flow of zero.

The pressure and flow rate data obtained for two channel heights of 20 and 50  $\mu\text{m}$  are shown in Figs. 17 and 18. These results indicate that adding an additional electrode array to the top cover of the micropump can significantly increase both the pumping pressure and flow rate for a given applied potential. As shown in Fig. 18, a micropump with the top and bottom electrodes is able to pump nearly three times as much when compared to a micropump with bottom electrodes only. Thus, it can be concluded that adding an array of electrodes to the top

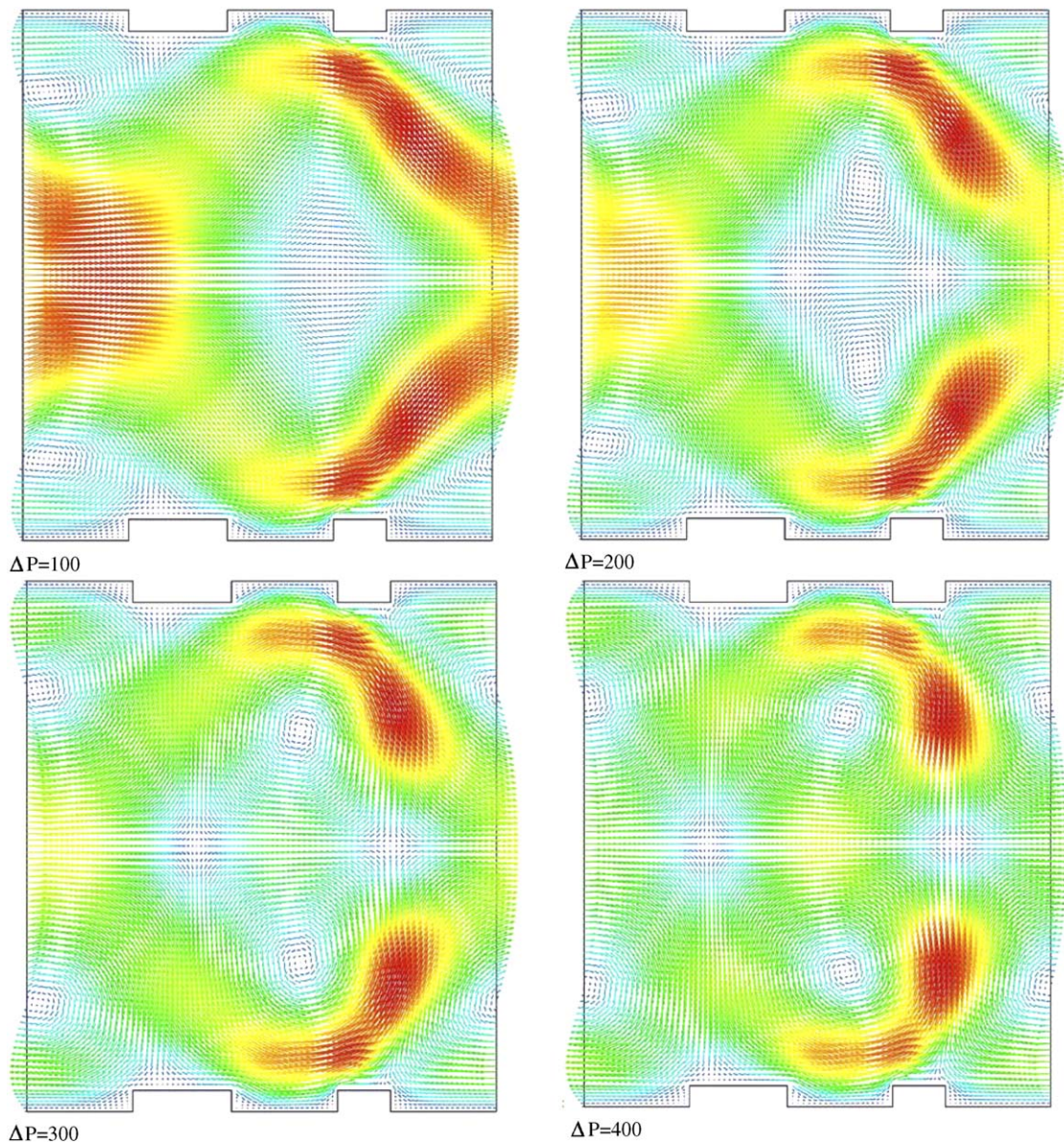


Fig. 16. Local velocity profiles at various pressures for a channel height of 50  $\mu\text{m}$  with top and bottom electrodes.

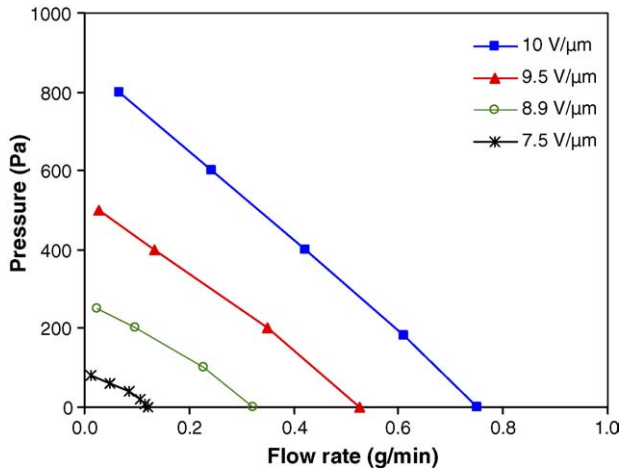


Fig. 17. Pumping pressure vs. mass flow rate at various electric fields for a channel height of 20  $\mu\text{m}$  with top and bottom electrodes.

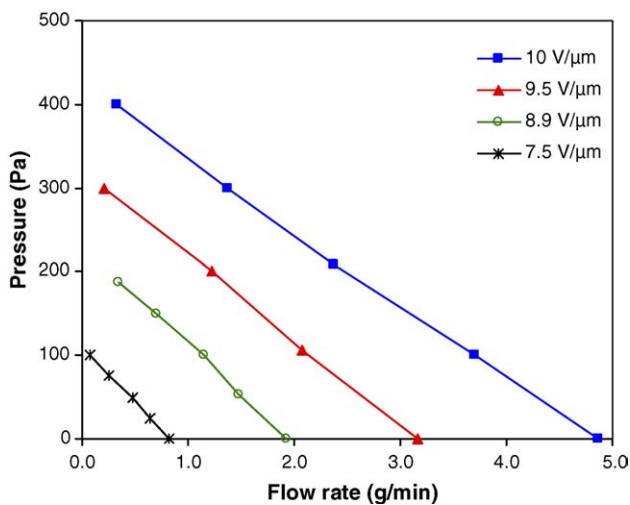


Fig. 18. Pumping pressure vs. mass flow rate at various electric fields for a channel height of 50  $\mu\text{m}$  with top and bottom electrodes.

cover could be used as a way to obtain higher flow rates and pumping power without significantly complicating the fabrication process.

## 5. Conclusions

A computational model has been developed for investigating microscale EHD pumping. The model was first validated with experimental data and then used to perform parametric simulations of an EHD micropump. The effects of applied voltage, electrode gap, stage gap,  $d/g$  ratio, channel height, and electrode configuration were investigated. It was found that for a given channel height there is an optimum  $d/g$  ratio at which the flow rate is maximum. Additionally, it was shown that adding an additional array of electrodes to the top cover could significantly increase both the pumping pressure and flow rate. The results of this simulation study can provide new insight into behavior of ion-drag EHD pumps which cannot be easily obtained from experimental results. The simulation results

presented here are believed to be the first published work to numerically model EHD pumping. This work is ongoing. Our future work will focus on developing a 3D numerical model to simulate EHD pumping with three-dimensional saw-tooth microstructures.

## Acknowledgements

This work is partially supported by a grant from the South Carolina NASA/EPSCoR Program.

## References

- [1] N.T. Nguyen, X.Y. Huang, T.K. Chuan, MEMS-micropumps: a review, *J. Fluids Eng. Trans. ASME* 124 (2002) 384–392.
- [2] D.J. Laser, J.G. Santiago, A review of micropumps, *J. Micromech. Microeng.* 14 (2004) R35–R64.
- [3] J. Darabi, H. Wang, Emerging opportunities and challenges in micropumps, in: *Proceedings of the IMECE2002 ASME International Mechanical Engineering Congress and Exposition, IMECE2002-39586*, 2002.
- [4] O.M. Stuetzer, Ion-drag pumping, *J. Appl. Phys.* 31 (1) (1959) 136–146.
- [5] O.M. Stuetzer, Ion-drag pressure generation, *J. Appl. Phys.* 30 (7) (1959) 984–993.
- [6] W.F. Pickard, Ion-drag pumping I theory, *J. Appl. Phys.* 34 (1963) 246–250.
- [7] W.F. Pickard, Ion-drag pumping II experiments, *J. Appl. Phys.* 34 (1963) 251–258.
- [8] A.M. Sharbaugh, G.M. Walker, The design and evaluation of an ion drag dielectric pump to enhance cooling in a small oil-filled transformer, in: *Proceedings of the IEEE-IAS-Annual Meeting, Mexico City, 1983*, pp. 1161–1165.
- [9] J.M. Crowley, G.M. Graham, J.C. Chato, Selecting a working fluid to increase the efficiency and flow rate of an EHD pump, *IEEE Trans. Ind. Appl.* 26 (1) (1984) 42–49.
- [10] S.F. Bart, L.S. Tavrow, M. Mehregany, J.H. Lang, Microfabricated electrohydrodynamic pumps, *Sens. Actuators A* 21 (1) (1990) 1937.
- [11] A. Tochter, H. Sandmaier, An electrohydrodynamic pump, *IEEE Micro Electro Mechanical Systems: An Investigation of Micro Structures, Sensors, Actuators, Machines and Robots*, 11–14 February 1990, pp. 99–104.
- [12] G. Fuhr, R. Hagedorn, T. Muller, W. Benecke, Microfabricated electrohydrodynamic (EHD) pumps for liquids of higher conductivity, *JMEMS* 1 (3) (1992) 1416.
- [13] J. Seyed-Yagoobi, J.E. Bryan, J.A. Castaneda, Theoretical analysis of ion-drag pump, *IEEE Trans. Ind. Appl.* 31 (3) (1995) 469–476.
- [14] G. Barbini, G. Coletti, Influence of electrode geometry on ion-drag pump static pressure, *IEEE Trans. Dielectrics Electrical Insulation* 2 (1995) 1100–1105.
- [15] V.V. Gogosov, K.V. Polyansky, V.A. Polyansky, G.A. Shaposhnikova, A.A. Vartanyan, Modeling of nonstationary processes in channels of EHD pump, *J. Electrostat.* 34 (2–3) (1995) 245–262.
- [16] C.C. Wong, D.R. Adkins, D. Chu, Development of a Micropump for Microelectronic Cooling, *American Society of Mechanical Engineers, Dynamic Systems and Control Division (Publication) DSC, Micro-Electro-Mechanical Systems (MEMS)*, vol. 59, 1996, pp. 239–244.
- [17] S.H. Ahn, Y.K. Kim, Fabrication and experiment of planar micro ion-drag pump, *Sens. Actuators A* 70 (1998) 1–5.
- [18] M.K. Bologna, I.A. Kozhukhar, I.V. Cojvevicov, Electrohydrodynamic pumps, in: *IEEE International Conference on Conduction and Breakdown in Dielectric Liquids, ICDL, 1999*, pp. 546–547.
- [19] A.I. Zhakin, S.A. Lunev, Theory of net-EHD pump, in: *IEEE International Conference on Conduction and Breakdown in Dielectric Liquids, ICDL, 1999*, pp. 544–545.

- [20] K. Asano, K. Yatsuzuka, Fundamental study of EHD pump with needle-cylinder electrodes, Conference on Electrical Insulation and Dielectric Phenomena (CEIDP), Annual Report, vol. 2, 1999, pp. 785–788.
- [21] J. Darabi, M. Rada, M.M. Ohadi, J. Lawler, Design, fabrication, and testing of an electrohydrodynamic ion-drag micropump, *J. Microelectromech. Syst.* 11 (6) (2002) 684–690.
- [22] Kojevnikov, I.V., Motorin, O.V., Bologa, M.K., Kojevnikova, A.I., Optimization of the electrohydrodynamic pump, Conference on Electrical Insulation and Dielectric Phenomena (CEIDP), Annual Report, 2002, pp. 204–207.
- [23] H. Yanada, S. Hakama, T. Miyashita, N. Zhang, An investigation of an ion drag pump using a needle-mesh electrode configuration, *Proc. Inst. Mech. Eng., Part C: J. Mech. Eng. Sci.* 216 (2002) 325–335.
- [24] M. Watanabe, J.M. Zheng, A. Hara, H. Shirai, T. Hirai, A pumping technique using electrohydrodynamic flow inside a gel, *IEEE Trans. Dielectrics Electrical Insulation* 10 (2003) 181–185.
- [25] M. Watanabe, H. Shirai, T. Hirai, Liquid–liquid two-layer electrohydrodynamic flow system, *Sens. Actuators B: Chem.* 94 (2003) 267–270.
- [26] L.J. Yang, J.M. Wang, Y.L. Huang, The microion drag pump using indium-tin-oxide (ITO) electrodes to resist aging, *Sens. Actuators A: Phys.* 111 (2004) 118–122.
- [27] M. Watanabe, A. Hara, T. Hirai, Gel-coated electrodes for an ion drag pump, *IEEE Trans. Dielectrics Electrical Insulation* 11 (2004) 139–143.
- [28] J. Darabi, H. Wang, Development of an electrohydrodynamic injection micropump and its potential application in pumping fluids in cryogenic cooling systems, *J. Microelectromech. Syst.* 14 (4) (2005) 747–755.

## Biographies

**Jeff Darabi** is an assistant professor of Mechanical Engineering at the University of South Carolina, Columbia. He received his M.S. and Ph.D. degrees in Mechanical Engineering from the University of Maryland, College Park in 1997 and 1999, respectively. His active research interests are in the areas of microelectromechanical systems (MEMS), microfluidics, BioMEMS, and chip-integrated micro cooling systems. Dr. Darabi has pioneered several novel micropumps and microcooling devices for high heat flux electronic cooling applications. He is currently active in the development of chip-integrated micro cooling systems where he holds a related patent, dielectrophoretic manipulation of DNA, electrospray ionization, and micropumps for cooling spatially separate electronic components. Dr. Darabi is a member of ASME, IEEE, and ASHRAE. He is the recipient of the ASHRAE New Investigator Award (2005–2006), the Outstanding Research Team at the SCAMP Undergraduate Research Conference (2004), Pi Tau Sigma Mechanical Engineering Professor of the Year Award (2002), the Homer Addams Award (1999), the University of Maryland Outstanding Student Service Award (1999), and ASHRAE Grant-in-aid Fellowship (1995–1996, and 1998–1999).

**Curtis Rhodes** received his B.S., M.S., and Ph.D. degrees from Texas A&M University, University of Pittsburgh, and Carnegie Mellon University. He is currently a Professor of Mechanical Engineering at the University of South Carolina. He has previously worked at Los Alamos Scientific Laboratory and Jet Propulsion Laboratory. His research is in heat transfer and fluid mechanics of two-phase flows, natural convection, and thermal radiation.